

# Mapping stellar kinematics across the Galactic bar: HST measurements of proper motions in 35 fields. \*

S. Kozłowski<sup>1†</sup>, P. R. Woźniak<sup>2</sup>, S. Mao<sup>1</sup>, M. C. Smith<sup>3</sup>, T. Sumi<sup>4</sup>,  
W. T. Vestrand<sup>2</sup> and Ł. Wyrzykowski<sup>5</sup>

<sup>1</sup> Jodrell Bank Observatory, The University of Manchester, Macclesfield, Cheshire SK11 9DL, UK

<sup>2</sup> Los Alamos National Laboratory, MS-D466, Los Alamos, NM 87545, USA

<sup>3</sup> Kapteyn Institute, PO Box 800, 9700 AV Groningen, the Netherlands

<sup>4</sup> Princeton University Observatory, Princeton, NJ 08544, USA

<sup>5</sup> Institute of Astronomy, University of Cambridge, Madingley Road, Cambridge CB3 0HA, UK

Accepted 2006 April 26. Received 2006 April 26; in original form 2006 March 22

## ABSTRACT

We present a proper motion mini-survey of 35 fields in the vicinity of Baade window,  $(l, b) = (1^\circ, -4^\circ)$ , sampling roughly a  $5 \times 2.5$  deg region of the Galactic bar. Our second epoch observations collected with the ACS/HRC instrument on board the Hubble Space Telescope were combined with the archival WFPC2/PC images. The resulting time baselines are in the range of 4–8 years. Precise proper motions of 15,863 stars were determined in the reference frame defined by the mean motion of stars with magnitudes between  $I_{F814W} = 16.5 - 21.5$  along the line of sight. We clearly detect small gradients in proper motion dispersions  $(\sigma_l, \sigma_b) \sim (3.0, 2.5)$  mas yr<sup>-1</sup>, and in the amount of anisotropy  $(\sigma_l/\sigma_b \sim 1.2)$ . Both the longitude dispersion  $\sigma_l$  and its ratio to the vertical motion  $\sigma_b$  increase toward the Galactic plane. The decline of the anisotropy ratio  $\sigma_l/\sigma_b$  toward the minor axis of the bulge is mostly due to increasing  $\sigma_b$ . We also find, for the first time, a significant negative covariance term in the transverse velocity field  $\sigma_b/(\sigma_l\sigma_b) \simeq -0.10$ . Our results extend by a factor of  $\sim 15$  the number of the Galactic bar fields with good proper motion dispersions.

**Key words:** galactic dynamics - Stars: proper motion, dispersion  
gravitational lensing - Galaxy: bar, bulge, disc

## 1 INTRODUCTION

The Milky Way appears to be a typical spiral galaxy with a disk and bulge. While our unique inside view of the Galaxy helps to understand the galactic structure in general, it also makes it more difficult to identify structures such as bars. The case for existence of a bar at the Galactic centre – first proposed by de Vaucouleurs (1964) – is easier to make knowing that bars are common in external galaxies.

There is now conclusive evidence that the Galactic bulge is of a barred type. The longitude asymmetry of the COBE photometric maps (Blitz & Spergel 1991;

Dwek et al. 1995), high optical depths to gravitational microlensing (Zhao, Spergel & Rich 1995), asymmetric star counts (Stanek et al. 1994; Babusiaux & Gilmore 2005), non-circular gas kinematics (de Vaucouleurs 1964), and triaxiality of the stellar velocity field (Zhao, Spergel & Rich 1994; Zhao, Rich & Biello 1996) have all been interpreted as signatures of the Galactic bar. Unfortunately, the size and precise orientation of the bar are still being debated. Recently Benjamin et al. (2005) found that the infra-red star counts collected by the Spitzer Space Telescope are best explained assuming a bar with a half-length  $4.4 \pm 0.5$  kpc placed at a  $\sim 44^\circ$  angle to the Sun–Galactic center line. Most previous studies prefer a bar at  $\sim 20^\circ$  extending out to  $\sim 3.5$  kpc (e.g. Gerhard 2001). Such apparently conflicting evidence may be an indication that the inner Galaxy hides even more complicated structures. A secondary bar (Alard 2001; Babusiaux & Gilmore 2005) and a ring (Sevenster & Kalnajs 2001) have been suggested, since these

\* Based on observations made with the NASA/ESA Hubble Space Telescope, obtained from the data archive at the Space Telescope Science Institute. STScI is operated by the Association of Universities for Research in Astronomy, Inc. under NASA contract NAS 5-26555.  
† E-mail: simkoz@jb.man.ac.uk

features are also evident in many other spiral galaxies (e.g. Erwin & Sparke 1999).

Binney (2005) discussed the progress of the dynamical modeling techniques in the context of major observational advances expected from a future space mission GAIA. The three approaches to constructing a self-consistent dynamical Galaxy model are the Schwarzschild method (Zhao, Spergel & Rich 1994; Häfner et al. 2000), the torus modelling method (see Binney 2005 for details) and  $N$ -body simulations with particle weights determined by the “made-to-measure” algorithm (Syer & Tremaine 1996). The first Galactic bar model employing the latter method was built by Bissantz et al. (2004). Neither of these techniques can fully address the structure of the inner Galaxy without constraints on stellar kinematics. The refinement of the models is limited largely by the scarcity of good proper motion and radial velocity measurements. Bissantz et al. (2004), for example, compared kinematic predictions of their model with the data for just two lines of sight. A handful of samples published since the pioneering photographic work of Spaenhauer et al. (1992) is not enough to remove the non-uniqueness of the model parameters.

In a study based on two lines of sight Kuijken & Rich (2002) have demonstrated that high quality relative proper motions can be obtained with a relatively modest investment of time using the Hubble Space Telescope (HST). At the resolution of the Wide Field Planetary Camera 2 (WFPC2) instrument the required time baseline is only a few years. The HST archive contains a number of images suitable as the first epoch data, so the tedious part of accumulating the baseline can be avoided entirely. Most of these fields are centred around microlensing events discovered by the MA-CHO collaboration (e.g. Popowski et al. 2005). Using a similar concept to that of Kuijken & Rich (2002), we carried out a mini-survey of proper motions in 35 of the available MA-CHO fields to study the kinematics of microlensed sources and of the general stellar populations. Here we present the measurement techniques and results for the general stellar population in these 35 lines of sight.

## 2 HST IMAGES AND DATA REDUCTION

The log of the HST observations used in our proper motion mini-survey is given in Table 1. The first epoch images (selected from the HST archive<sup>1</sup>) were all taken with the WFPC2/PC camera, and cover the time interval 1996–2000. The second epoch data come from our own SNAP program (cycle 13; proposal ID 10198) and were collected in 2004 and 2005 using the High Resolution Channel (HRC) of the Advanced Camera for Surveys (ACS). Our SNAP survey was optimized toward high execution rates and, therefore, we only requested F814W observations to keep the required target visibility as low as possible. Both PC and HRC detectors cover a similar field of view ( $25'' \times 29''$  and  $35'' \times 35''$ , respectively) and have comparable pixel scales (27 versus 45.5 mas). There were no restrictions on the telescope roll angle during ACS observing. While the latter relaxed condition decreased the number of possible proper motion de-

terminations, it greatly improved scheduling opportunities. Most of the subsequent analysis for each of the 35 fields is based on a pair of good quality F814W ( $I$ -band) images constructed by stacking all suitable data for a given epoch. In some cases, the first epoch data included F555W ( $V$ -band) images that allowed us to construct color-magnitude diagrams (CMDs). We also re-analyzed the two fields previously studied by Kuijken & Rich (2002), increasing to 37 the total number of the Galactic bulge fields considered here.

### 2.1 Image reductions

The basic reductions of the ACS images, i.e. de-biasing, dark frame subtraction, flat-fielding, and cosmic-ray removal, were performed on-the-fly by the standard HST data processing pipeline. The pipeline also takes care of dithering, cosmic-ray splits and geometric corrections using the Multidrizzle software (Koekemoer et al. 2002), which in turn uses the Drizzle routines (Fruchter & Hook 2002). Our ACS observations employed a generous 4-point dithering pattern combined with a 2-way cosmic-ray split, providing the final drizzled images with high S/N ratio, excellent dynamic range and highly reliable cosmic-ray rejection. In case of the first-epoch WFPC2 images we utilized the standard HST data products for individual exposures, and then used the `drizzle` task of the IRAF package to correct the geometric distortions. For cosmic-ray cleaning, registering and combining these corrected images we developed dedicated IRAF scripts. The quality of our final cross-instrument astrometry is limited by the larger pixel size, as well as the lower S/N ratio and number of the individual first epoch PC frames available for stacking by comparison to the ACS data (see §3).

### 2.2 Object catalogs and PSF fitting

The instrumental positions and magnitudes of the field objects were measured using the IRAF task `starfind`, an improved version of `daofind` that fits Gaussian profiles to stellar images. The combined images from both WFPC2/PC and ACS/HRC detectors have a well sampled point-spread-function (PSF) with the full-width-at-half-maximum (FWHM) of stellar images, correspondingly, 2.4 and 2.8 pixels. Our PSF fits were restricted within the area of the Airy disc (3.0 and 2.0 pixel radius for PC and HRC data respectively), where the point source flux is well approximated by a Gaussian model. Outside the Airy disc the PSFs show a variety of shapes, including rings, possible diffraction spikes and bright spots in case of high S/N objects. These features can mimic stars and need to be carefully considered during object cross-identification. We imposed a minimum separation of  $3 \times \text{FWHM}$  between any two sources detected in the same image to ensure that there are essentially no spurious objects in the final source lists. The loss of number statistics due to the accidental rejection of the actual stars in tight groups is insignificant. In fact, the centroid measurements for objects in the wings of other stars are notoriously unreliable and best avoided. The minimum separation cut also helps in cross identification of objects between the two epochs (§3), since the expected intrinsic object shifts may reach  $\sim 2$  PC pixels.

<sup>1</sup> <http://archive.stsci.edu/hst/>

**Table 1.** Log of the HST observations.

MACHO field	RA	Dec	First epoch			Second epoch		
			Year	F814W exp.	F555W exp.	Prop. ID	Year	F814W exp.
108-C	18:00:01.276	-28:27:41.23	1996.82	6 × 260 s		6756	2005.16	4 × 260 s
119-C	18:03:03.010	-30:09:56.50	1996.82	6 × 260 s		6756	2005.15	4 × 260 s
119-D	18:04:24.825	-30:05:58.94	1996.82	6 × 260 s		6756	2004.78	4 × 260 s
120-A	18:07:26.441	-29:39:34.22	1996.82	6 × 260 s		6756	2005.15	4 × 260 s
167-A	18:13:32.154	-26:31:10.33	1996.82	6 × 260 s		6756	2005.16	4 × 260 s
101-C	18:07:32.649	-27:31:35.60	1997.47	6 × 260 s		6756	2005.15	4 × 260 s
95-BLG-11	18:04:37.239	-30:12:11.45	1996.67	6 × 260 s		6756	2005.16	4 × 260 s
96-BLG-17	18:06:09.107	-27:53:38.59	1996.81	6 × 260 s		6756	2005.17	4 × 260 s
119-A	18:03:35.789	-29:42:01.26	1996.68	6 × 160 s	2 × 400 s	6756	2005.14	4 × 160 s
95-BLG-7	18:13:29.298	-26:13:58.12	1998.84	2 × 40 s	3 × 40 s	7431	2005.46	4 × 40 s
95-BLG-10	17:58:16.011	-29:32:10.86	1997.82	2 × 40 s	3 × 40 s	7431	2004.66	4 × 40 s
95-BLG-13	18:08:47.038	-27:40:47.25	1999.45	2 × 40 s	3 × 40 s	7431	2005.12	4 × 40 s
95-BLG-14	18:01:26.308	-28:31:14.03	2000.45	2 × 40 s	3 × 40 s	7431	2005.40	4 × 40 s
95-BLG-19	18:11:32.487	-27:45:26.99	1998.49	2 × 40 s	3 × 40 s	7431	2005.44	4 × 40 s
97-BLG-18	18:03:15.254	-28:00:14.06	1998.59	2 × 40 s	3 × 40 s	7431	2005.31	4 × 40 s
104-C	18:03:34.050	-28:00:18.94	1998.73	2 × 40 s	3 × 40 s	7431	2005.43	4 × 40 s
104-D	18:03:29.024	-28:00:30.99	1998.80	2 × 40 s	3 × 40 s	7431	2005.45	4 × 40 s
108-A	18:00:25.866	-28:02:35.24	1998.80	2 × 40 s	3 × 40 s	7431	2005.16	4 × 40 s
128-B	18:07:18.624	-28:59:29.83	1998.49	2 × 30 s	3 × 40 s	7431	2005.37	4 × 30 s
104-B	18:03:09.046	-28:01:45.25	1999.45	2 × 40 s	3 × 40 s	7431	2005.39	4 × 40 s
128-A	18:06:57.621	-29:00:55.15	1999.33	2 × 40 s	3 × 40 s	7431	2005.49	4 × 40 s
94-BLG-3	17:58:25.300	-29:47:59.50	1997.82	2 × 40 s	3 × 40 s	7431	2005.48	4 × 40 s
94-BLG-4	17:58:36.766	-30:02:19.27	1997.82	2 × 40 s	3 × 40 s	7431	2005.16	4 × 40 s
95-BLG-36	18:07:20.775	-27:24:09.69	1998.80	2 × 40 s	3 × 40 s	7431	2005.39	4 × 40 s
95-BLG-37	18:04:34.452	-28:25:33.46	1999.43	2 × 40 s	3 × 40 s	7431	2004.67	4 × 40 s
95-BLG-38	17:59:41.851	-28:12:10.31	1998.81	2 × 40 s	3 × 40 s	7431	2005.33	4 × 40 s
95-BLG-41	18:02:06.332	-28:50:45.26	1999.46	2 × 40 s	3 × 40 s	7431	2005.44	4 × 40 s
96-BLG-14	18:05:15.421	-27:58:25.01	1997.83	2 × 40 s	3 × 40 s	7431	2004.67	4 × 40 s
96-BLG-4	18:06:11.954	-28:16:52.77	1998.79	2 × 26 s	3 × 40 s	7431	2004.82	4 × 26 s
97-BLG-38	18:04:06.083	-27:48:26.25	1998.51	2 × 40 s	3 × 40 s	7431	2004.63	4 × 40 s
97-BLG-24	18:04:20.253	-27:24:45.28	1998.35	2 × 40 s	3 × 40 s	7431	2005.49	4 × 40 s
96-BLG-5	18:05:02.497	-27:42:17.23	1999.45	4 × 160 s	2 × 400 s	8490	2005.12	4 × 160 s
98-BLG-6	17:57:32.812	-28:42:45.41	2000.48	2 × 100 s	2 × 260 s	8654	2004.73	4 × 100 s
97-BLG-41	17:56:20.691	-28:47:41.97	2000.47	4 × 100 s	4 × 160 s	8654	2004.62	4 × 100 s
99-BLG-22	18:05:05.281	-28:34:41.69	2001.77	4 × 400 s	4 × 400 s	9307	2005.16	4 × 400 s

The final object catalogs were converted to the VEGA magnitude system (Girardi et al. 2002 and references therein) and the astrometric transformations to the Galactic (l, b) coordinates were established using the World Coordinate System (WCS) headers of the ACS images. Our estimated S/N ratios for object fluxes are based on propagated errors in pixel counts that account for photon statistics.

### 3 ESTIMATING TRANSVERSE MOTIONS OF THE GALACTIC BULGE STARS

Absolute astrometry is difficult in the crowded Galactic bulge fields. Until we can establish a sample of extragalactic objects (e.g. spectroscopically confirmed QSOs in the catalogue of candidates by Sumi et al. 2005) shining through the low extinction windows, the only readily available reference velocity in the Galactic bulge is the mean velocity of stars along the line of sight. Notice, however, that the second order moments of proper motions are unaffected by the choice of our reference frame. In this analysis we use the magnitude- and distance-selected samples to investigate the spatial de-

pendence of the covariance matrix of the transverse velocity field across the Galactic bar.

#### 3.1 Relative proper motions and their dispersions

Having measured the instrumental positions of stars on both the first and the second epoch images, we tied the WFPC2/PC positions to the ACS/HRC pixel grid. The object shifts  $\Delta l$  and  $\Delta b$  in the Galactic coordinates between the two epochs could then be calculated using the WCS information from the ACS headers. We cross-correlated the positions of a few hundred stars in the magnitude range  $16.5 < I_{F814W} < 21.5$  to obtain the coordinate transformation between two pixel grids, which is approximated by a third order polynomial. Stars brighter than  $I_{F814W} = 16.5$  were often saturated while those with  $I_{F814W} > 21.5$  were too faint to have useful S/N ratios, particularly for the fields with short exposures (Table 1). Our procedure for cross-identifying stars starts from matching the first 20 objects (out of  $\sim 50$  brightest stars with  $17 < I_{F814W} < 18$ ) using the triangle algorithm (Groth 1986; Woźniak 2000). The initial low-order fit is then iteratively refined. A star with a

transverse velocity of 100 km/s at the distance of 8 kpc will move by 26.4 mas, or roughly one ACS/HRC pixel, assuming a 10 year baseline. Accordingly, we adopted a tolerance radius of 100 mas for the final matching.

After geometrically aligning and transforming object positions to the Galactic ( $l, b$ ) coordinates, we folded the data with the time baseline and estimated all components of the transverse velocity tensor, i.e. dispersions  $\sigma_l, \sigma_b$  and the normalized covariance  $C_{lb} \equiv \sigma_{lb}/(\sigma_l\sigma_b)$ . The sample of stars used to trace the kinematic parameters of the Galactic bulge was limited to the magnitude range  $18.0 < I_{F814W} < 21.5$ , i.e. dominated by the bulge main sequence population near the turn-off point. This puts all lines of sight (with data sets of the varying depth and dynamic range) on a more common footing. However, as already noted by Kuijken & Rich (2002), the results are insensitive to the details of the magnitude cuts.

### 3.2 Astrometric errors

The  $1\sigma$  centroid errors from PSF fitting (per coordinate) can be estimated from the S/N ratio (SNR):

$$\delta \simeq \gamma \times \frac{\text{FWHM}}{\text{SNR}}, \quad (1)$$

where  $\gamma = 0.6$  for a Gaussian PSF model and the FWHM is in pixels (see e.g. Kuijken & Rich 2002). We tested this prescription by stacking independent subsets of images taken at a single epoch. Similarly to Kuijken & Rich (2002), we find that Equation 1 is an excellent representation of the actual astrometric uncertainties in our data, with the exception of the brightest stars, for which a constant systematic contribution of 0.025 pixel is required. Consequently, we used Equation 1 with the systematic term added in quadrature to estimate the astrometric errors and their contribution to the apparent proper motion dispersions. The formulas for estimating  $\sigma_l, \sigma_b$  and their errors corrected for the measurement variance can be found in Spaenhauer et al. (1992). Throughout this paper we use bootstrapped uncertainties of the sample statistics (from 1000 trials) that turned out to be slightly more conservative than analytical formulas. The estimated intrinsic dispersions reported in § 4 are 5–10% lower compared to the raw values. The cross term  $C_{lb}$  need not be corrected, as long as the errors in  $l$  and  $b$  are uncorrelated. None of our conclusions depend on the precise value or even the presence of this correction.

The limiting S/N ratio for a useful detection in our analysis is about 10 and corresponds to a  $I_{F814W} \simeq 21.5$  mag star in the combined image of two 40-second WFPC2/PC exposures. The same star will be detected at S/N  $\sim 20$  in the lowest quality ACS stack (four 40-second frames). The shortest time baseline in our data is 3.388 years, and the typical  $1\sigma$  astrometric uncertainties for a 21.5 mag star are  $\sim 7.2$  and  $\sim 2.1$  mas in the first and the second epoch images respectively. In this worst case scenario, the proper motion can be measured to an accuracy  $2.5 \text{ mas yr}^{-1}$ . The images for the first eight fields in Table 1 have relatively long exposure times, so the resulting proper motion errors are only  $\sim 0.1 \text{ mas yr}^{-1}$  for bright stars and  $\sim 0.3 \text{ mas yr}^{-1}$  for the faintest stars in those samples, with a systematic error of 0.025 pixel (c.f. discussion following equation (1)).

## 4 RESULTS

The results are given in Table 2 and plotted in Figs. 1 and 2. Proper motions for individual stars are available online<sup>2</sup>. After presenting our measurements we check for consistency with two other published data sets (§ 4.3). A more detailed discussion and comparison to the results of Kuijken & Rich (2002) follows in § 5.

### 4.1 Proper motion dispersions

The spatial dependence of proper motion dispersions  $\sigma_l, \sigma_b$  is shown in Fig. 1. Recall that at a distance of 8 kpc, a velocity of  $100 \text{ km s}^{-1}$  implies a proper motion of  $2.64 \text{ mas yr}^{-1}$ . The most visible trends are in  $\sigma_l(b)$  and  $\sigma_b(l)$  that tend to increase closer to the Galactic plane and the Galactic centre. Both gradients are weak, but clearly present. From a simple straight line fit we find:

$$\sigma_l = 0.16 \pm 0.04 \times b + 3.38 \pm 0.13, \quad (2)$$

$$\sigma_b = -0.09 \pm 0.02 \times l + 2.62 \pm 0.06. \quad (3)$$

Consequently,  $\sigma_b$  increases from 2.1 to 2.6  $\text{mas yr}^{-1}$ , or by about 20%, as the longitude  $l$  varies from 5.5 to 0.5 deg. Similarly,  $\sigma_l$  changes from 2.6 to 3.2  $\text{mas yr}^{-1}$  between  $b = -4.5$  and  $-2$  deg. It is intriguing that the last data point around  $b \approx -2$  deg has the lowest dispersion ( $\sigma_l$ ) measured for all fields (see the top right panel in Fig. 1), but the value is still marginally consistent with the observed scatter. There is no other indication of the intrinsic variations on the field-to-field scale. The distributions of  $\sigma_l(l)$  and  $\sigma_b(b)$  are flat within the scatter from random errors and projection effects in the presence of gradients.

### 4.2 Anisotropy and covariance

In Fig. 2 we plot the ratio and the correlation coefficient (covariance of the velocity field) of  $\sigma_l$  and  $\sigma_b$  as a function of location in the bulge. There is a significant level of anisotropy, i.e.  $\sigma_l/\sigma_b > 1$ , throughout the covered area. Moreover, the velocity distribution shows a tendency to become more isotropic for lines of sight approaching the Galactic centre at a roughly fixed latitude  $b$ . This is a reflection of the increase in  $\sigma_b$  with approximately constant  $\sigma_l$  (§ 4.1). The trend of more anisotropy toward the Galactic plane is also driven primarily by one of the dispersions ( $\sigma_l$ ), but it is more difficult to see. Part of the reason for this is the narrow range of  $b$  covered by the data. The formal fits give:

$$\sigma_l/\sigma_b = 0.05 \pm 0.01 \times l + 1.08 \pm 0.03, \quad (4)$$

$$\sigma_l/\sigma_b = 0.03 \pm 0.03 \times b + 1.27 \pm 0.08. \quad (5)$$

The estimates of the covariance term from Table 2 (plotted in Fig. 2) are all negative and scatter uniformly in the range  $-0.20 < C_{lb} < -0.02$ . This indicates that in our Galactic bulge fields the stellar motions in directions parallel and perpendicular to the plane are significantly anti-correlated. An observational bias that would account for this anti-correlation has to operate in a similar way over

<sup>2</sup> <http://www.jb.man.ac.uk/~simkoz/dispersions/>

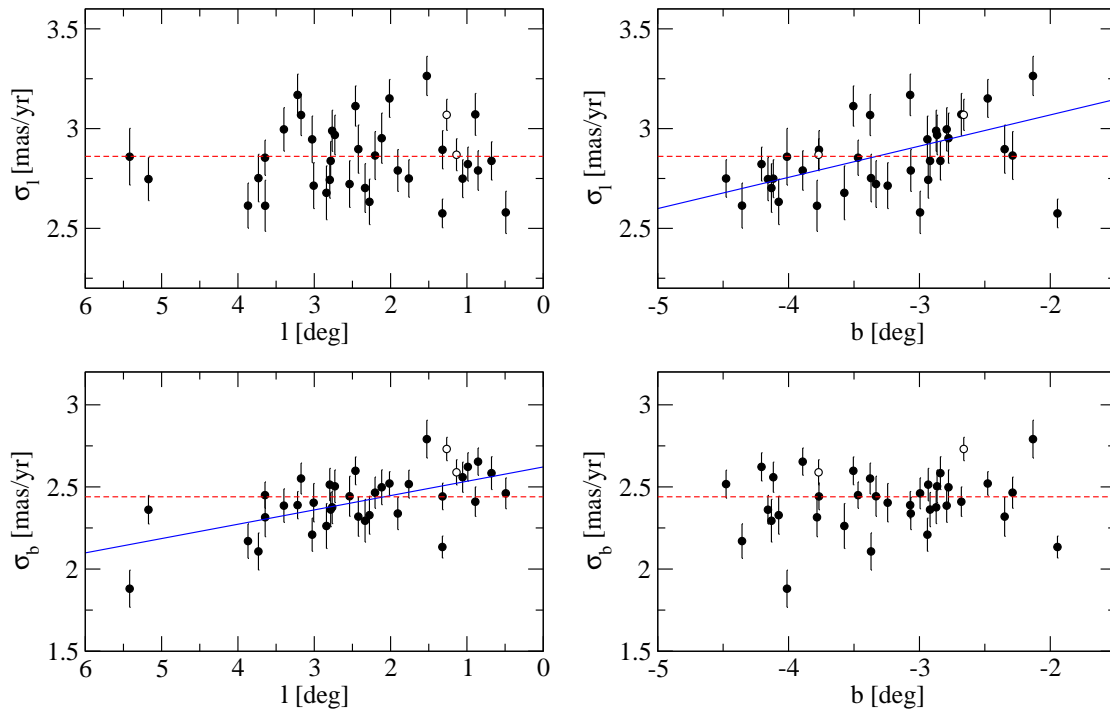


**Figure 1.** Spatial dependence of proper motion dispersions  $\sigma_l$  and  $\sigma_b$  in Galactic coordinates for our turn-off point dominated sample in the Galactic bulge (Table 2 and §4). The two open circles are for the Baade window and Sagittarius-I fields from Kuijken & Rich (2002). The lines show linear regressions (solid) and weighted means (dashed) of the data. For the top right panel, the rightmost data point was not used in the fit.

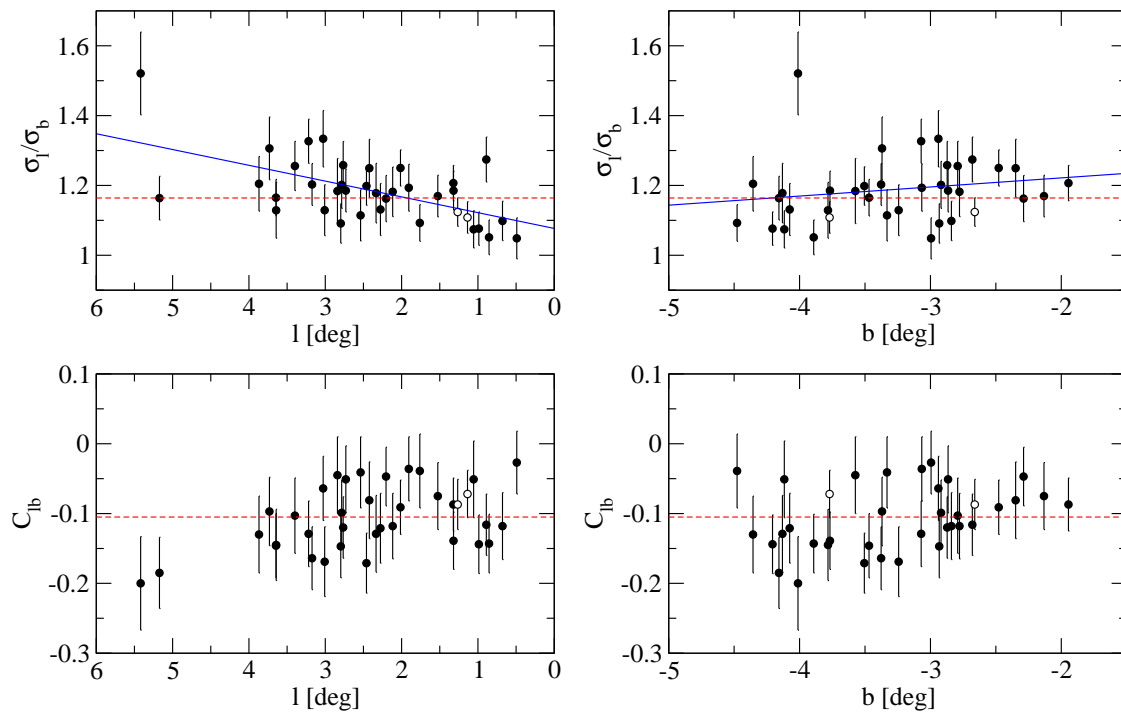


**Figure 2.** Similar to Fig. 1 but for the anisotropy ratio  $\sigma_l/\sigma_b$  and covariance term  $C_{lb} \equiv \sigma_{lb}/(\sigma_l\sigma_b)$ .

**Table 2.** Results of our proper motion mini-survey. The dispersions  $\sigma_l, \sigma_b$  and the dimensionless correlation coefficient  $C_{lb}$  were measured for 35 lines of sight in the Galactic bulge (l, b). The time baseline  $\Delta t$  and the number of stars  $N_{\text{stars}}$  used to estimate the kinematics are also given.

Field name	l [deg]	b [deg]	$\sigma_l$ [ mas yr <sup>-1</sup> ]	$\sigma_b$ [ mas yr <sup>-1</sup> ]	$C_{lb}$	$\Delta t$ [yr]	$N_{\text{stars}}$
101-C	3.65	-3.47	2.85 ± 0.09	2.45 ± 0.08	-0.15 ± 0.05	7.683	445
104-B	2.73	-2.87	2.97 ± 0.10	2.50 ± 0.10	-0.05 ± 0.05	5.941	407
104-C	2.80	-2.93	2.74 ± 0.09	2.51 ± 0.10	-0.15 ± 0.04	6.706	482
104-D	2.79	-2.92	2.84 ± 0.10	2.36 ± 0.10	-0.10 ± 0.05	6.649	437
108-A	2.42	-2.35	2.90 ± 0.12	2.32 ± 0.12	-0.08 ± 0.06	6.360	396
108-C	2.02	-2.48	3.15 ± 0.10	2.52 ± 0.07	-0.09 ± 0.04	8.345	615
119-A	1.32	-3.77	2.89 ± 0.10	2.44 ± 0.08	-0.14 ± 0.04	8.458	471
119-C	0.85	-3.89	2.79 ± 0.10	2.65 ± 0.08	-0.14 ± 0.04	8.339	459
119-D	1.06	-4.12	2.75 ± 0.10	2.56 ± 0.09	-0.05 ± 0.06	7.962	420
120-A	1.76	-4.48	2.75 ± 0.09	2.52 ± 0.09	-0.04 ± 0.05	8.339	397
128-A	2.28	-4.08	2.63 ± 0.11	2.33 ± 0.12	-0.12 ± 0.05	6.165	357
128-B	2.33	-4.13	2.70 ± 0.12	2.29 ± 0.13	-0.13 ± 0.06	6.881	338
167-A	5.17	-4.16	2.75 ± 0.11	2.36 ± 0.09	-0.18 ± 0.05	8.345	317
94-BLG-3	0.68	-2.84	2.84 ± 0.10	2.58 ± 0.10	-0.12 ± 0.05	7.654	496
94-BLG-4	0.49	-3.00	2.58 ± 0.11	2.46 ± 0.09	-0.03 ± 0.04	7.341	413
95-BLG-10	0.89	-2.68	3.07 ± 0.10	2.41 ± 0.09	-0.12 ± 0.04	6.840	487
95-BLG-11	0.99	-4.21	2.82 ± 0.09	2.62 ± 0.09	-0.14 ± 0.04	8.493	443
95-BLG-13	3.64	-3.78	2.61 ± 0.13	2.31 ± 0.12	-0.14 ± 0.05	5.672	309
95-BLG-14	2.12	-2.78	2.95 ± 0.13	2.50 ± 0.11	-0.12 ± 0.05	4.950	463
95-BLG-19	3.87	-4.36	2.61 ± 0.11	2.17 ± 0.10	-0.13 ± 0.06	6.952	300
95-BLG-36	3.73	-3.37	2.75 ± 0.12	2.11 ± 0.11	-0.10 ± 0.05	6.587	376
95-BLG-37	2.54	-3.33	2.72 ± 0.12	2.44 ± 0.12	-0.04 ± 0.05	5.238	442
95-BLG-38	2.20	-2.29	2.87 ± 0.12	2.46 ± 0.10	-0.05 ± 0.04	6.526	474
95-BLG-41	1.91	-3.07	2.79 ± 0.10	2.34 ± 0.10	-0.04 ± 0.05	5.980	450
95-BLG-7	5.42	-4.01	2.86 ± 0.14	1.88 ± 0.11	-0.20 ± 0.07	6.616	265
96-BLG-14	3.01	-3.24	2.71 ± 0.12	2.40 ± 0.12	-0.17 ± 0.05	6.833	373
96-BLG-17	3.17	-3.38	3.07 ± 0.10	2.55 ± 0.09	-0.16 ± 0.04	8.364	557
96-BLG-4	2.84	-3.57	2.68 ± 0.14	2.26 ± 0.14	-0.04 ± 0.06	6.027	329
96-BLG-5	3.22	-3.07	3.17 ± 0.10	2.39 ± 0.08	-0.13 ± 0.05	5.670	535
97-BLG-18	2.77	-2.87	2.99 ± 0.10	2.38 ± 0.10	-0.12 ± 0.04	6.713	433
97-BLG-24	3.40	-2.79	3.00 ± 0.11	2.39 ± 0.10	-0.10 ± 0.05	7.115	398
97-BLG-38	3.03	-2.94	2.95 ± 0.12	2.21 ± 0.10	-0.06 ± 0.05	6.118	395
97-BLG-41	1.32	-1.95	2.58 ± 0.07	2.13 ± 0.07	-0.09 ± 0.04	5.145	612
98-BLG-6	1.53	-2.13	3.26 ± 0.10	2.79 ± 0.12	-0.07 ± 0.05	4.252	670
99-BLG-22	2.46	-3.50	3.11 ± 0.10	2.60 ± 0.09	-0.17 ± 0.04	3.388	493
KR-BW <sup>a</sup>	1.14	-3.77	2.87 ± 0.08	2.59 ± 0.08	-0.07 ± 0.03	6.048	694
KR-SgrI	1.26	-2.66	3.07 ± 0.08	2.73 ± 0.07	-0.09 ± 0.04	5.960	752

<sup>a</sup> KR-BW and KR-SgrI are the Baade window and the Sagittarius-I field from Kuijken & Rich (2002)

a large range of instrumental settings. For example, a serious concern is a presence of preferred telescope orientations. Indeed, for about half of our fields the relative roll angle between the two compared observations falls in a narrow range of 25 deg. The other half, however, is spread over all possible orientations and still shows about the same covariance. The skewness of the ACS focal plane cannot be the cause of the observed correlation, because the measurements in both Kuijken & Rich (2002) fields use only WFPC2/PC data and yet they perfectly agree with the rest of the  $C_{lb}$  values. We also investigated several other possibilities, we found no explanation for this result other than a true correlation between  $\mu_l$  and  $\mu_b$ . Taking a field with a relatively low S/N ratio in our data and assuming perfectly correlated errors in  $\mu_l$  and  $\mu_b$ , the expected covariance is only  $C_{lb} \sim 0.02$ .

There is a slight hint in Fig. 2 that  $C_{lb}$  may vary with the longitude, although this impression seems to rely on the two points farthest from the bulge minor axis ( $\simeq 5.3$  deg in the left panel of Fig. 2) that fall below the rest of the data.

### 4.3 Comparisons with previous work

#### 4.3.1 OGLE-II proper motion catalogue

Sumi et al. (2004) used large number statistics of the OGLE-II database (Udalski et al. 1997) to derive relative proper motions of  $\gtrsim 5 \times 10^6$  stars in the Galactic bulge region from hundreds of observations covering a 4-year baseline. The OGLE-II catalogue is a valuable resource for kinematic studies of bright stars like red clump giants that are

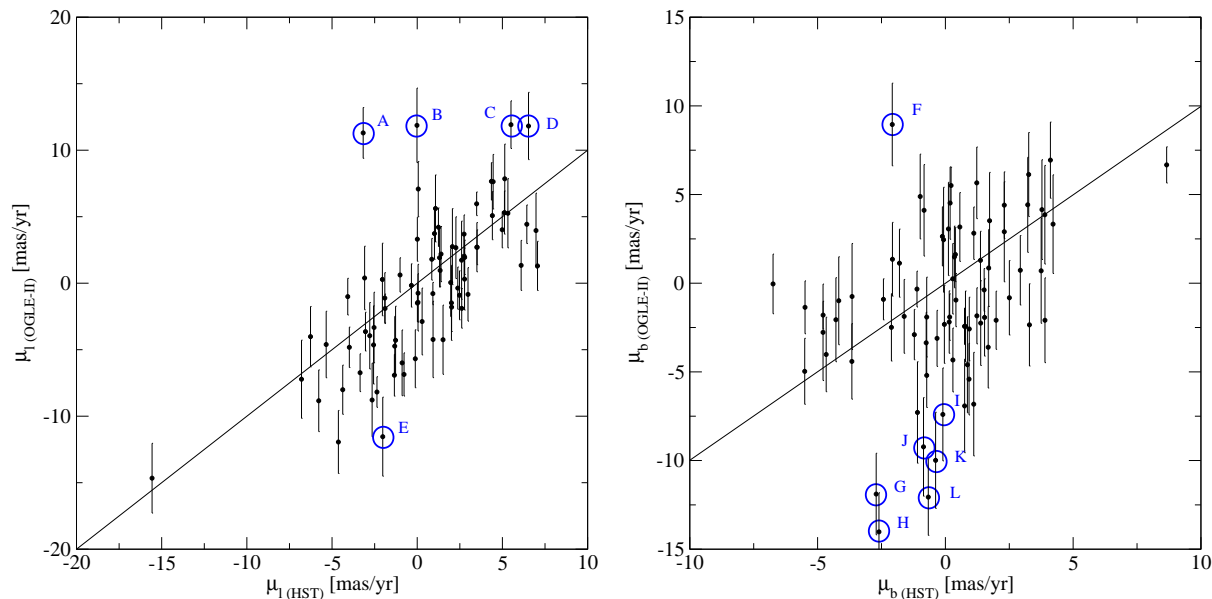


**Figure 3.** Comparison between our HST measurements and the ground based OGLE-II data for bright stars from the catalogue of Sumi et al. (2004). There are 77 stars covered by our observations that have catalogue errors  $3 \text{ mas yr}^{-1}$  or better in Sumi et al. Significant discrepancies (marked by alphabets) are caused by blending (c.f Fig. 4). The solid lines indicate the two measurements (ground-based and from the HST) are equal.

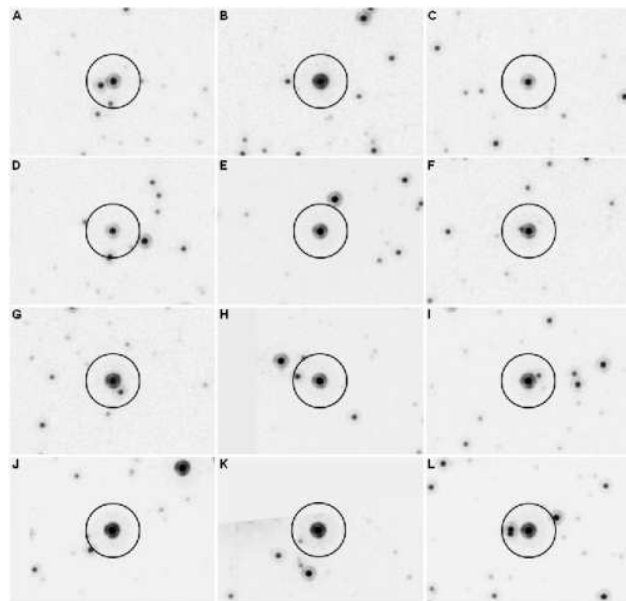
relatively free of the source confusion effects. However, at the  $1.3''$  FWHM seeing of the ground based OGLE-II images, a random red clump giant star still has a few per cent probability of being blended with another unresolved star. It is instructive to cross-validate the results of Sumi et al. (2004) and our high-resolution HST measurements against each other.

Out of 35 program fields in Table 1, 15 are covered by the OGLE-II proper motion catalogue. In our HST sample we found 77 stars for which the OGLE-II catalogue proper motion error is  $\leq 3 \text{ mas yr}^{-1}$ . The two data sets were compared star by star after adjusting for an arbitrary zero point of the proper motion scale. The results are plotted in Fig. 3 and show a good overall agreement of our measurements with Sumi et al. (2004). All significant outliers were labeled and checked for blending. Fig. 4 demonstrates that virtually all these substantial discrepancies are linked to the presence of an unresolved companion within  $\sim 1''$  of the primary object.

#### 4.3.2 Kuijken & Rich (2002)

Our approach to measuring the positions and proper motions of stars (§ 2.2) is somewhat simpler than the method used by Kuijken & Rich (2002). The latter study utilized the images from the WFPC2/WF chips and had to accommodate a strong under-sampling of the PSF. In contrast, our use of the WFPC2 data was limited to the critically sampled images from the PC detector. The second epoch ACS/HRC images have four times the PSF sampling of the WF images, so we could take advantage of the conventional PSF fitting techniques.

Regardless, in order to eliminate the possibility of a hidden error we re-analysed the PC data in both fields studied by Kuijken & Rich (2002) using our tools. Table 3 shows the

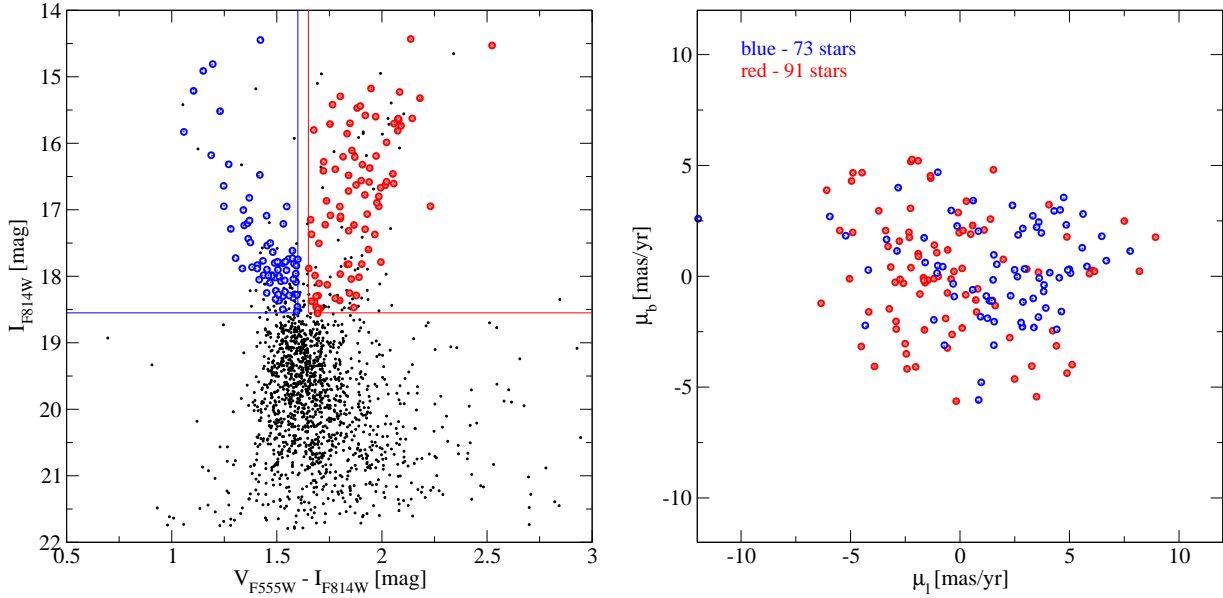
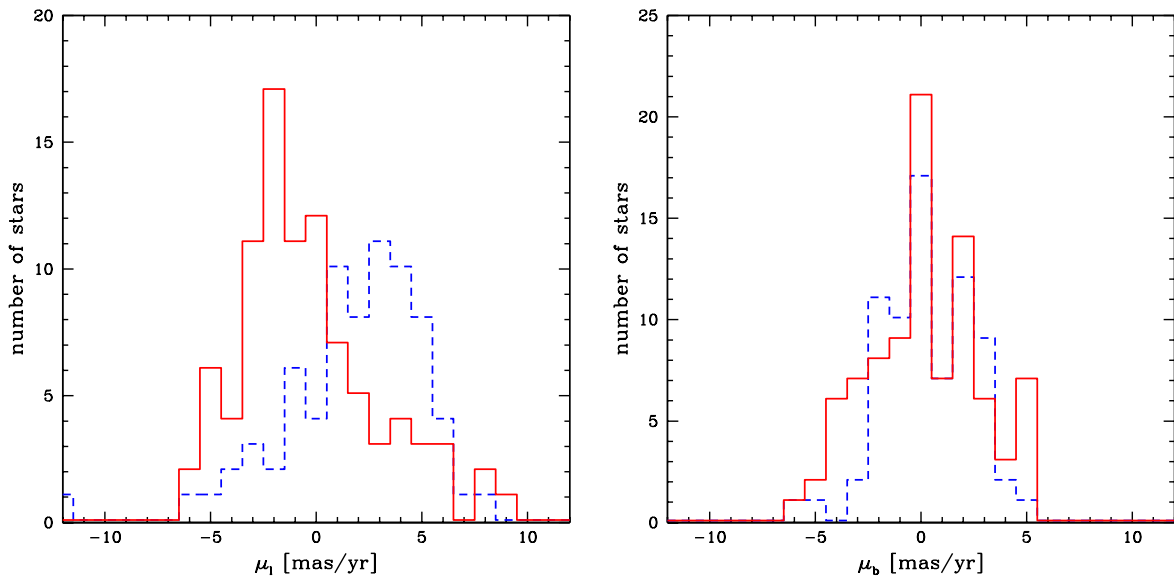


**Figure 4.** Cutout HST images for the outliers marked by alphabets in Fig. 3. All significant outliers in Fig. 3 can be linked to source confusion and flux blending. The dark circles have a diameter of 1 arc second.

results of this comparison. The agreement between the two sets of measurements is remarkably close despite significant differences in the sample size and the adopted selection criteria. This also confirms that our results are not significantly affected by several subtle instrumental effects that can potentially influence astrometric work with the HST images (e.g. Kuijken & Rich 2002 and references therein).

**Table 3.** Proper motion dispersions from Kuijken & Rich (2002) compared with the results of our reanalysis of the same data

Field	l	b	This work			Kuijken & Rich (2002)		
			$\sigma_l$	$\sigma_b$	$N_{\text{stars}}$	$\sigma_l$	$\sigma_b$	$N_{\text{stars}}$
BW	1.14	-3.77	$2.87 \pm 0.08$	$2.59 \pm 0.08$	694	$2.91 \pm 0.06$	$2.51 \pm 0.05$	1076
Sgr-I	1.27	-2.66	$3.07 \pm 0.08$	$2.73 \pm 0.07$	752	$3.10 \pm 0.06$	$2.73 \pm 0.05$	1388

**Figure 5.** Color-magnitude diagram (CMD; left) and relative proper motions (right) for stars in three nearly coincident stellar fields from Table 2: 97-BLG-18, 104-C and 104-D. The red and blue stars above the turn-off point show the kinematics characteristic of the bulge and disk populations, respectively.**Figure 6.** Histograms of relative proper motions of the red (solid line) and blue (dashed line) samples from Fig. 5 The blue disk stars “rotate in front” of the Galactic bulge parallel to the plane.



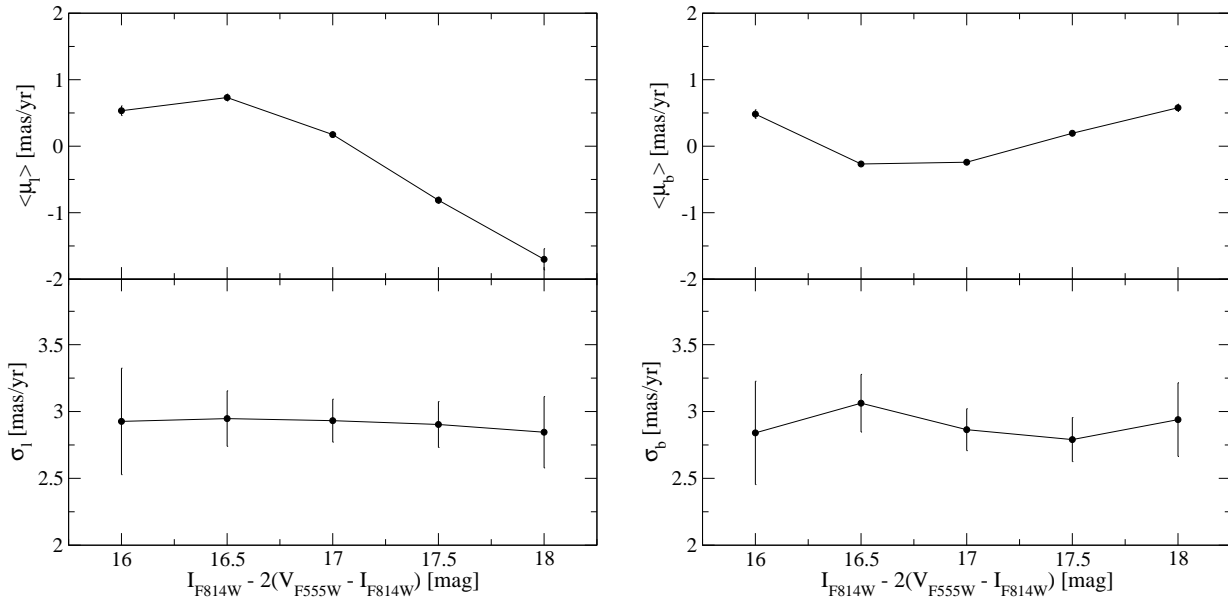


**Figure 7.** Average relative proper motions and dispersions of stars in the Baade Window in bins of  $M^* \equiv I_{F814W} - 2(V_{F555W} - I_{F814W})$ , an approximate distance indicator.

## 5 DISCUSSION

### 5.1 Distance and population trends

The study of Kuijken & Rich (2002) focused on cleaning the Galactic bulge population and removing the contamination by the bluer disk stars. Above the bulge turn-off point, the stellar colors alone are sufficient to separate the blue disk main sequence from the red giants, subgiants and clump giants. The size of our fields is generally too small to provide useful statistics of bright stars above turn-off point, and good color information is only available for about 1/3 of the lines of sight. However, three of the fields in Table 1 with useful colors (97-BLG-18, 104-C and 104-D) are close to each other and were combined in order to look for a kinematic distinction between the Galactic disk and bulge populations. Figs 5 and 6 show that in the frame of reference of a mean star (of any color), the longitude proper motions of the blue disk stars are biased toward positive values, while the red bulge stars tend to have more negative  $\mu_l$ . The blue and red samples were selected, correspondingly, using conditions  $(V - I) < 1.65$  and  $(V - I) > 1.7$ . This effect was previously observed by Sumi et al. (2005) and by Kuijken & Rich (2002) in their two fields with multi-epoch WFPC2 data and there is little doubt that it is due to the blue disk stars “rotating in front” of the red bulge stars.

Kuijken & Rich (2002) also devised an approximate distance measure:

$$M^* = I_{F814W} - 2(V_{F555W} - I_{F814W}) \quad (6)$$

chosen to remove the slope of the main sequence in the color-magnitude diagram. In Fig. 7 we present the average proper motions and their dispersions for the Baade window in bins of  $M^*$ . As expected, with an increasing depth along the line of sight, the kinematic signature gradually changes from that characteristic of the disk stars, to the one typical for the bulge. In the Kuijken & Rich (2002) data this trend continues to very faint stars that are likely on the far side

of the bulge, and if so, it constitutes a “rotation curve” of the bulge. The colors for our fields are generally of lower S/N ratio or nonexistent, and do not allow to see this much detail.

### 5.2 Stellar velocity ellipsoid of the Galactic bar

A detailed modeling of the measurements in Table 2 is beyond the scope of this paper. Here we only comment on possible directions and new possibilities.

Zhao, Rich & Biello (1996) interpreted the bulge anisotropy in terms of the rotation support of the Galactic bulge and related the ratio  $\sigma_l/\sigma_b$  directly to the level of flattening of the light density distribution. They also concluded that the value  $\sigma_l/\sigma_b = 1.10\text{--}1.15$  observed in Baade window (l, b)  $\sim (1^\circ, -4^\circ)$ , with which our measurements are consistent, can be explained by rigid rotation. The presence of any disk stars, however, will also contribute rotational broadening to  $\sigma_l$ . Since in the vicinity of our fields the disk fraction increases closer to the plane, it follows that the measured gradient from equation (2) could be due to the disk contamination. The changes of skewness in the  $\mu_l$  distribution tend to support this (see Fig. 6). Another possibility is that the rotation rate of the bulge actually increases at lower  $|b|$ , as found by Izumiura et al. (1995) from the radial velocities of 124 SiO masers in the Galactic bulge. It has been observed that for giants in Baade window the metal-poor stars display more spread in the vertical motion and less anisotropy when compared to metal-rich samples (Zhao, Spergel & Rich 1994; Zhao, Rich & Biello 1996). Both of these metallicity dependencies are quite steep, so it is likely that the gradient from equation (3) is related to a changing mix of populations with more metal-poor stars closer to the Galactic bulge minor axis.

We are not aware of any previous detections of the cross terms in the Galactic bulge velocity field except the report by Zhao, Spergel & Rich (1994) of a significant ver-

tex deviation between the radial and longitudinal motions from  $C_{r1}$ . That result is based on a photographic sample of  $\sim 200$  K and M giants from Spaenhauer et al. (1992). We note that the latter sample actually shows a hint of a slightly negative covariance between  $\mu_l$  and  $\mu_b$  (c.f. Fig. 1 of Zhao, Spergel & Rich 1994). The superb resolution of HST enabled very significant detections of the  $C_{1b}$  cross term in many fields. The non-diagonal elements of the velocity tensor are crucial to determining the dominant orbit families, the importance of streaming motions and the need for the intrinsic anisotropy versus solid body rotation in the Galactic bulge (Zhao, Spergel & Rich 1994; Zhao, Rich & Biello 1996; Häfner et al. 2000). Häfner et al. (2000) published detailed calculations of  $C_{1b}$  for several lines of sight at positive longitudes including Baade window ( $1^\circ, -4^\circ, C_{1b} = 0.04$ ), and two other: ( $8.4^\circ, -6^\circ, C_{1b} = 0.15$ ) and ( $1.21^\circ, -1.67^\circ, C_{1b} = 0.04$ ). Taken at face value these predictions are roughly of the same magnitude as the results from § 4, but have the opposite sign. For a proper comparison with dynamical models like the ones in Häfner et al. (2000) and Bissantz et al. (2004) we need to wait until the calculations are folded with the appropriate selection functions, since our measurements are based on substantially deeper data than most of the previous samples.

## 6 SUMMARY AND CONCLUSIONS

The main results of our proper motion mini-survey are: (1) high quality proper motion measurements for hundreds of stars in 35 lines of sight across the Galactic bar, (2) establishing the presence of spatial gradients in dispersions  $\sigma_l, \sigma_b$  and the amount of anisotropy  $\sigma_l/\sigma_b$ , and (3) the first reliable detection of the covariance term  $C_{1b}$  of the transverse velocity tensor. We cross-validated our measurements with the ground based OGLE-II data of Sumi et al. (2004) and a benchmark study of Kuijken & Rich (2002). The observed slow rise of  $\sigma_l$  toward the Galactic plane is likely due to the increasing disk contamination and/or a possible gradient in the bulge rotation speed. The increase in  $\sigma_b$  toward the minor axis of the bulge is accompanied by the decreasing ratio  $\sigma_l/\sigma_b$  and possibly results from increasing fraction of metal-poor stars. Another possibility is that  $\sigma_b$  increases due to the larger surface density of stars at low  $l$  (closer to the Galactic centre). We clearly detect the covariance term  $C_{1b} \sim -0.10$  that implies a significant tilt of the Galactic bulge velocity ellipsoid with respect to the Galactic plane. Using the same procedures as in Binney & Merrifield (1998, §10.3.2), we find the tilt is roughly equal to  $-24^\circ$ .

The data presented in this paper provide qualitatively new constraints on dynamical models of the inner Galaxy and dramatically improved number statistics. Furthermore, it may be possible in the near future to augment our proper motion samples with the distance and metallicity estimates. As shown by Kuijken & Rich (2002), deep color-magnitude diagrams can supply sufficiently accurate distance information to effectively isolate the bulge population. In order to maximize the discriminating power of model comparisons the focus should be on extending the coverage to negative longitudes and locations further from the Galactic centre.

## ACKNOWLEDGMENTS

We thank Profs. Bohdan Paczyński, Ian Browne and Drs. Vasily Belokurov, Wyn Evans and Nicholas Rattenbury for helpful comments.

Support to P.W. for proposal SNAP-10198 was provided by NASA through a grant from the Space Telescope Science Institute, which is operated by the Association of Universities for Research in Astronomy, Inc., under NASA contract NAS5-26555.

This work was partly supported by the European Community's Sixth Framework Marie Curie Research Training Network Programme, Contract No. MRTN-CT-2004-505183 "ANGLES", in particular S.K. through a studentship, L.W. through a PDRA, and S.M. through travel support.

M.C.S. acknowledges financial support from the Netherlands Organisation for Scientific Research (NWO).

## REFERENCES

- Alard, C., 2001, *A&A*, 379, L44
- Alcock, C., et al., 2000, *ApJ*, 541, 734
- Babusiaux, C., Gilmore, G., 2005, *MNRAS*, 358, 1309
- Benjamin, R. A., et al., 2005, *ApJ*, 630, L149
- Binney, J. J., 2005, preprint (astro-ph/0411229)
- Binney, J. J., Merrifield, M. R., 1998, *Galactic Astronomy* (Princeton University Press)
- Bissantz, N., Debattista, V. P., Gerhard, O., 2004, *ApJ*, 601, L155
- Blitz, L., Spergel, D. N., 1991, *ApJ*, 379, 631
- de Vaucouleurs, G., 1964, in Kerr, F., Rodgers, A., eds, *Proc. IAU Symp. 20, The Galaxy and the Magellanic Clouds*. Australian Academy of Sciences, Canberra, p. 195
- Dwek, E., et al., 1995, *ApJ*, 445, 716
- Erwin, P., Sparke, L. S., 1999, *ApJ*, 521, L37
- Fruchter, A. S., Hook, R. N., 2002, *PASP*, 114, 144
- Gerhard, O., 2001, in *ASP Conf. Ser. 230, Galaxy Disks and Disk Galaxies*, eds. J. G. Funes, & E. M. Corsini (San Francisco: ASP), 21
- Girardi, L. et al., 2002, *A&A*, 391, 195
- Groth, E. J., 1986, *AJ*, 91, 1244
- Häfner, R., Evans, N. W., Dehnen, W., Binney, J., 2000, *MNRAS*, 314, 433
- Izumiura, H., et al., 1995, *ApJS*, 98, 271
- Koekemoer, A. M., Fruchter, A. S., Hook, R. N., Hack, W., 2002, *The 2002 HST Calibration Workshop*, 2002, 339
- Kuijken, K., Rich, R. M., 2002, *AJ*, 124, 2054
- Popowski, P., et al., 2005, *ApJ*, 631, 879
- Sevenster, M. N., Kalnajs, A. J., 2001, *AJ*, 122, 885
- Spaenhauer, A., Jones, B. F., Whitford, A. E., 1992, *AJ*, 103, 297
- Sumi, T., et al., 2004, *MNRAS*, 348, 1439
- Sumi, T., et al., 2005, *MNRAS*, 356, 331
- Syer, D., Tremaine, S., 1996, *MNRAS*, 282, 223
- Stanek, K. Z., Mateo, M., Udalski, A., Szymański, M., Kaluzny, J., & Kubiak, M., 1994, *ApJ*, 429, L71
- Udalski, A., Kubiak, M., Szymański, M., 1997, *Acta Astronomica*, 47, 319
- Woźniak, P., 2000, *Acta Astronomica*, 50, 421
- Zhao, H.S., Spergel, D. N., Rich, R. M., 1994, *AJ*, 108, 2154
- Zhao, H.S., Spergel, D. N., Rich, R. M., 1995, *ApJ*, 440, L13

Zhao, H.S., Rich, R. M., Biello, J., 1995, ApJ, 470, 506